

Article

Self-Assembled Multinuclear Complexes for Cobalt(II/III) Mediated Sensitized Solar Cells

Edoardo Marchini ^{1,*}, Stefano Caramori ^{1,*} , Rita Boaretto ¹, Vito Cristino ¹, Roberto Argazzi ², Alessandro Niorettini ¹ and Carlo Alberto Bignozzi ¹ 

¹ Department of Chemical, Pharmaceutical, and Agricultural Sciences, University of Ferrara, Via L. Borsari 46, 44121 Ferrara, Italy; bar@unife.it (R.B.); crsvti@unife.it (V.C.); nrtlsn@unife.it (A.N.); g4s@unife.it (C.A.B.)

² CNR-ISOF c/o Department of Chemical, Pharmaceutical and Agricultural Sciences, University of Ferrara, Via L. Borsari 46, 44121 Ferrara, Italy; agr@unife.it

* Correspondence: mrcdrd@unife.it (E.M.); cte@unife.it (S.C.); Tel.: +39-0532-455-146 (S.C.)

Abstract: In this work, we designed a tetranuclear self-assembled dye **4** (2Z907-Ag⁺-(Ru(TMAM))) exploiting a combination of the antenna effect and positively-charged groups designed to repel the oxidized form of cationic cobalt redox mediators, in order to reduce recombination and increase the efficiency of dye sensitized solar cells (DSSCs). Charge transfer and excited dynamics were probed by photoelectrochemical and photophysical measurements. The sensitized cell performance, recorded with a [Co(bpy)₃]^{3+/2+} redox mediator and PEDOT counter electrode, showed an improvement when passing from **Z907** to the multinuclear systems. The enhancement of the efficiency compared to **Z907** resulted mainly from a superior steric and electrostatic shielding determined by the simultaneous presence of long alkyl chains and quaternary ammonia ion units in the architecture of **4**.

Keywords: DSSC; silver ions; shielding; repulsion; antenna effects; n-type sensitization



Citation: Marchini, E.; Caramori, S.; Boaretto, R.; Cristino, V.; Argazzi, R.; Niorettini, A.; Bignozzi, C.A. Self-Assembled Multinuclear Complexes for Cobalt(II/III) Mediated Sensitized Solar Cells. *Appl. Sci.* **2021**, *11*, 2769. <https://doi.org/10.3390/app11062769>

Academic Editor: Dong-Won Kim

Received: 30 January 2021

Accepted: 13 March 2021

Published: 19 March 2021

Publisher's Note: MDPI stays neutral with regard to jurisdictional claims in published maps and institutional affiliations.



Copyright: © 2021 by the authors. Licensee MDPI, Basel, Switzerland. This article is an open access article distributed under the terms and conditions of the Creative Commons Attribution (CC BY) license (<https://creativecommons.org/licenses/by/4.0/>).

1. Introduction

Titania based dye sensitized solar cells (DSSCs), developed starting in the early 90s by Grätzel and O'Regan [1], represent a regenerative photoelectrochemical device type characterized by unique properties like transparency, low production cost, capability to harvest the diffuse light [2], and wide choice of color palette, which facilitate its building integration in both indoor and outdoor conditions [3,4]. The functioning of DSSCs is based on photoinduced charge transfer from a molecular sensitizer adsorbed on a porous semiconductor followed by its regeneration from a hole transporting phase, which commonly consists of a redox couple dissolved in an organic electrolyte. As a result, photon absorption results in the separation of electrons and holes, which are confined in two different phases (semiconductor for electrons and redox electrolyte for holes) where selective transport of the carriers should ideally occur. The best efficiencies are now obtained with fast redox shuttles like polypyridine cobalt [5] and copper [6] coordination compounds. The fruitful employment of these redox mediators is subordinated to the possibility of achieving an appropriate TiO₂ shielding against recombination involving the electron recombination with the oxidized mediator (namely Co(III) and Cu(II)). Donor- π -Acceptor (D- π -A) organic dyes like D35 and Y123 [7,8] take advantage from the steric hindrance of substituted triphenylamine groups to sterically screen the titania surface from the oxidized redox couple. The typical D- π -A architecture thus requires a careful design and a multistep synthetic route, which leads to highly expensive molecular species. On the other hand, Ru(II) complexes, despite containing a rare metal, are normally less expensive and more abundant than the best panchromatic D- π -A dyes. Other approaches to suppress recombination caused by fast redox couples involve either the co-adsorption of siloxanes [9] to saturate the surface sites uncovered by the dye sensitizers and exposed to the electrolyte, or the formation of insulating thin metal oxide layers including alumina and magnesia [10]. In this latter case, a careful

control of the thickness of the insulating layer is necessary in order to maintain an efficient charge injection by the dye. We thus investigated the possibility of realizing self-assembled molecular moieties that exploit Ag^+ as a bridging unit [11] between the NCS groups of sterically hindered **Z907** dyes (Figure 1a) and the cyano ligands of **1** ($[\text{Ru}(\text{TMAM})_2(\text{CN})_2]^{4+}$ (TMAM = bis-4,4'-bis(trimethylaminomethyl)2,2'-bipyridine)) (Figure 1b). This coordination compound, named **4** ($2\text{Z907-Ag}^+-(\text{Ru}(\text{TMAM}))$) (Figure 1c and Supplementary Materials (Figure S1f)) realizes a strong photon absorption and conversion in the 300–650 nm region thanks to the energy transfer (Figure 1d) from the $[\text{Ru}(\text{TMAM})_2(\text{CN})_2]^{4+}$ antenna [12] to the **Z907** complexes, which undergo photoinduced electron transfer. At the same time, we exploit the quaternary ammonium ions present on the TMAM ligand [13,14] and Ag^+ to add electrostatic repulsion to steric shielding of the surface against positively-charged Co(III) ions present in the electrolyte. This tetranuclear system comparatively outperforms **Z907** alone by a factor of ca. 2 when considering the energy conversion efficiency of dye sensitized solar cells based on the $[\text{Co}(\text{bpy})_3]^{3+/2+}$ redox mediator.

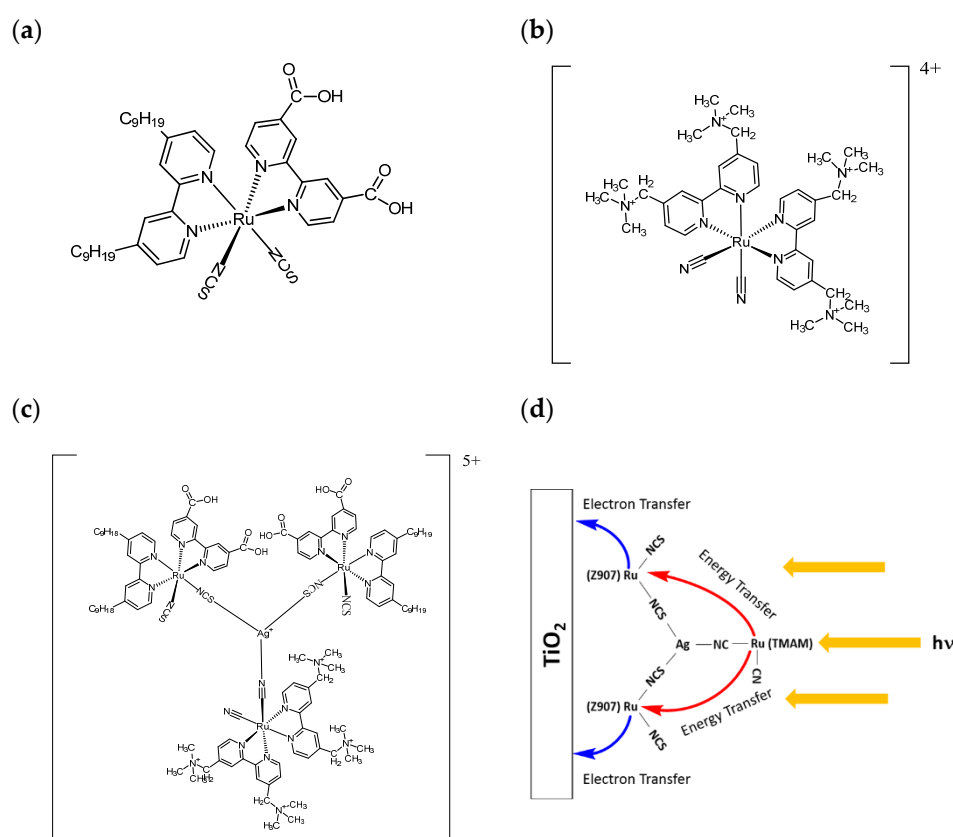


Figure 1. Schematic structure of: (a) **Z907**, (b) **1** ($\text{Ru}(\text{TMAM})$), (c) **4** ($2\text{Z907-Ag}^+-(\text{Ru}(\text{TMAM}))$); (d) energy transfer (red lines) and electron transfer (blue lines) processes involved in n-type sensitization.

2. Experimental Section

2.1. Materials

A total of 25% triethyl amine in H_2O , 65 wt.% HPF_6 , 99.995% lithium trifluoromethanesulfonate (LiOTf), $\text{NH}_4\text{PF}_6 \geq 98\%$, 96% 4-tert-Butylpyridine (TBPY), Dichloro(p-cymene) ruthenium(II) dimer, Sephadex LH-20, 97% Ethylenedioxythiophene (EDOT), Titanium(IV) isopropoxide ($\text{Ti}(\text{OiPr})_4$), Alconox, and solvents (anhydrous 99.8% Acetonitrile (ACN), ACS grade 2-propanol $\geq 99.8\%$, ACS grade absolute ethanol (EtOH), 99.9% 1-butanol, anhydrous 99.8% DMF (Dimethyl-formamide), 99.9 atom % D DMSO (dimethylsulfoxide)- d_6 , 99.9 atom % D acetone- d_6 , 99.9 atom % D acetonitrile- d_3) were bought from Sigma-Aldrich and used without further purification, $\text{LiTFSI} \geq 98\%$ was obtained from Alfa Aesar. $\text{LiClO}_4 \geq 99\%$ was purchased from Acros organics. FTO (Fluorine Tin Oxide) TEC-7 was bought from

NSG, and 18NR-T TiO₂ paste was purchased from Greatcell Solar. Surlyn 25 was supplied by Dyepower Consortium. ACS grade Silver nitrate was bought from Riedel-de Haën. 4,4'-bis(bromomethyl)-2,2'-bipyridine was already available from previous works and it was prepared according to the procedure in the literature [14,15]. [Co(bpy)₃](OTf)₂ (bpy = 2,2'-bipyridine and OTf = trifluoromethanesulfonate), [Co(bpy)₃](PF₆)₃, were prepared according to previous works [16]. [Ru(dcbH₂)(dnbpy)(NCS)₂] ((dcbH₂ = (4,4'-dicarboxy-2,2'-bipyridine) and dnbpy = (4,4'-dinonyl-2,2'-bipyridine)) were synthesized according to previous works [17]. ZrO₂ colloidal paste was also prepared following the literature [18].

2.2. Methods

Absorption spectra of solutions and of sensitized films were recorded in transmission mode with a Jasco V 570 at RT conditions against either a reference solvent or air respectively. ¹H and ¹³C NMR spectra were obtained with a Varian 400 MHz referring to the solvent residual peak.

Mass spectroscopy was carried out with a LCQ Duo Thermo Finnigan instrument equipped with an ESI (ElectroSpray Ionization) source. T = 160 °C, source voltage = 4.57 KV, capillary voltage = 10.32 V, flow rate = 25 µL/min.

Cyclic voltammetry analyses were obtained with a PGSTAT 302/N potentiostat in a three electrode-cell using glassy carbon or dyed films as working electrodes, a platinum wire as the counter electrode, and standard calomel electrode (SCE) as the reference.

Infrared spectra were recorded with a Bruker Vertex 70 FTIR (Fourier Transform Infrared spectrometer) in diffuse reflectance mode using the powder of each of the synthesized compounds dispersed in KBr against a blank KBr at RT under nitrogen flow.

J/V (Current density/voltage) curves of the DSSCs were obtained with a PGSTAT 302/N potentiostat setting under cyclic voltammetry mode. Illumination of the cells was achieved with an Abet sun simulator equipped with an AM1.5 G filter (the lamp irradiance was set to 100 mw/cm²). The photoaction spectra (IPCE (Incident Photon to Current Conversion Efficiency) vs. λ) were obtained under monochromatic illumination obtained by coupling a 300 W Luxtel xenon lamp with a Newport Cornerstone CS-260 monochromator. Illumination was orthogonal to the DSSCs via a Newport liquid light guide, illuminating a spot size of ca. 1.5 cm². A National Instruments PXI 4130 Source Measure Unit in a PXI-1033 chassis recorded the photocurrent from the cell under test, while a PXI-4065 Digital Multimeter simultaneously measured the voltage from a Thorlabs PDA100A-EC Si amplified detector monitoring part of the irradiating light reflected by a quartz beamsplitter.

Emission spectra were measured with an Edinburgh FS920 spectrofluorimeter equipped with a 450 W arc Xe lamp and a photomultiplier tube as detector.

Transient absorption and emission spectroscopy was carried out on both the fluid solution and on stained solid thin films in contact with 0.1 M LiClO₄/ACN (dyed TiO₂ and ZrO₂ films) with a time resolved spectrometer described elsewhere [19] at an excitation energy of 10 mJ/cm²/pulse. Within the time interval of interest, the S/N ratio of the traces was optimized by pre-amplifying the oscilloscope input signal with a suitable impedance.

Luminescence decay kinetics in the ns range were obtained by single-photon counting with TC-SPC apparatus (PicoQuant Picoharp 300) equipped with a nanosecond 460 nm LED source.

Electrochemical impedance spectroscopy (EIS) was carried out on illuminated DSSCs under open circuit potential (Voc) by applying a sinusoidal perturbation in the 10⁵–10^{−1} Hz range with an amplitude of 10 mV. The electron lifetimes were obtained from the $-Z''$ vs. frequency plot according to: $\tau = \frac{1}{2\pi f_{MAX}}$ where f_{MAX} represents the frequency of the maximum of the imaginary part of the impedance associated with the TiO₂/electrolyte interface.

The open circuit photovoltage decay (OCVD) experiments were collected in chronopotentiometry (zero current) mode. After a steady photopotential was attained, the illumination was suddenly turned off using a shutter and the photovoltage decay was sampled at

5×10^{-4} s intervals in an experiment with the total duration of 5 s. The lifetime τ_{el} was calculated according to $\tau_{el} = -\frac{kT}{e} \left(\frac{\partial V_{OC}}{\partial t} \right)^{-1}$.

2.3. Synthesis

4,4'-bis(trimethylaminomethyl)2,2'-bipyridine (TMAM) (Figure S1a): briefly, trimethylamine (54.47 mL) was added dropwise to a suspension of 4,4'-bis(bromomethyl)-2,2'-bipyridine (8.76 g 2.6 mmol) in ethanol (300 mL), the solution became light pink and a white solid was filtered off, washed with water, and dried [14,15]. (^1H NMR (400 MHz, Acetonitrile- d_3 , δ ppm): 8.88 (dd, $J = 5.0, 0.8$ Hz, 2H), 8.62 (dd, $J = 1.9, 0.8$ Hz, 2H), 7.60 (dd, $J = 5.0, 1.8$ Hz, 2H), 4.55 (s, 4H), 3.13 (s, 18H)). (Figure S2).

[Ru(TMAM) $_2$ Cl $_2$](PF $_6$) $_4$ (Figure S1b): the TMAM ligand (1 g 1.17 mmol) and the dimer dichloro(p-cymene)-ruthenium(II) (0.260 g 0.425 mmol) were dissolved in 35 mL of DMF, and heated with a microwave reactor at 150 °C for 25 min in an open flask fitted with a reflux condenser. DMF was evaporated to dryness and a dark violet solid was obtained. This intermediate complex was used without purification.

1 ([Ru(TMAM) $_2$ CN $_2$](TFSI) $_4$), (Ru(TMAM)) (Figure S1c): KCN (1 g, 15 mmol 80 eq) and Ru(TMAM) $_2$ Cl $_2$](PF $_6$) $_4$ (260 mg 0.19 mmol, 1 eq) were reacted in 13 mL of water in a microwave reactor for 5 min at 100 °C under atmospheric pressure. The product was first precipitated with an excess of LiTFSI, re-dissolved in the minimum amount of ACN, and re-precipitated by the addition of an excess volume of diethyl ether. The **1** (Ru(TMAM)) was loaded in a Sephadex LH-20 column and eluted with methanol. An orange solid was obtained following rotary evaporation. (^1H NMR (400 MHz, Acetone- d_6 , δ ppm): 10.00 (d, $J = 5.8$ Hz, 2H), 8.87 (s, 2H), 8.83 (s, 2H) 8.13 (d, $J = 5.7$ Hz, 2H), 7.99 (d, $J = 6.0$ Hz, 2H), 7.65 (dd, $J = 5.7, 1.7$ Hz, 2H), 5.06–4.86 (m, 8H), 3.49 (s, 18H), 3.39 (s, 18H). ^{13}C NMR (400 MHz, Acetone- d_6 , δ ppm): 157.63, 157.69, 155.55, 151.18, 149.65, 136.85, 135.92, 130.30, 127.09, 126.66, 66.92, 66.61, 52.91, 52.80) (Figures S3 and S4) (Figure S5, ESI-MS).

2 (Ru(TMAM)-Ag $^+$) (Figure S1d): This compound was obtained by mixing AgNO $_3$ and **1** (Ru(TMAM)) in a 1:1 ratio in either ethanol or methanol. (^1H NMR (400 MHz, DMSO- d_6 , δ ppm): 9.63 (1H), 8.68 (1H), 8.61 (1H), 7.92 (1H), 7.82 (1H), 7.47 (1H), 4.74 (2H), 4.55 (2H), 3.23 (9H), 3.08 (9H). ^{13}C NMR (400 MHz, DMSO- d_6 , δ ppm): 156.97, 156.26, 155.47, 150.75, 138.08, 137.09, 131.01, 130.68, 127.59, 127.06, 118.55, 66.62, 66.43, 56.46, 53.14) (Figures S6 and S7).

3 (ZZ907-Ag $^+$) (Figure S1e): This was obtained by mixing AgNO $_3$ and **Z907** in a stoichiometric 1:2 ratio in either methanol or ethanol. (^1H NMR (400 MHz, DMSO- d_6 , δ ppm): 9.44 (1H), 9.06 (2H), 8.93 (1H), 8.67 (1H), 8.52 (1H), 8.19 (1H), 7.79–7.73 (2H), 7.60 (1H), 7.27 (1H), 7.06 (1H), 2.85 (2H), 2.61 (2H), 1.75 (2H), 1.52 (2H), 1.32–1.15 (24H) 0.78 (6H). ^{13}C NMR (400 MHz, DMSO- d_6 , δ ppm): 165.77, 165.39, 159.47, 158.06, 157.87, 156.62, 153.90, 153.48, 153.08, 152.06, 151.56, 138.59, 137.84, 132.04, 131.15, 127.75, 126.56, 125.70, 124.18, 124.02, 123.43, 123.11, 35.14, 34.73, 31.76, 31.66, 30.28, 30.09, 29.42, 29.32, 29.28, 29.18, 29.14, 29.06, 22.57, 22.51, 14.43, 14.39) (Figures S8 and S9).

4 (ZZ907-Ag $^+$ -(Ru(TMAM))) (Figure S1f): This adduct was obtained by mixing **Z907** and **2** in a 2:1 ratio in either methanol or ethanol. (^1H NMR (400 MHz, DMSO- d_6 , δ ppm): 9.71 (1H), 9.42 (1H), 9.05 (2H), 8.93 (1H), 8.72–8.63 (3H), 8.52 (1H), 8.21 (1H), 7.91 (1H), 7.82 (1H), 7.77 (2H), 7.60 (1H), 7.45 (1H), 7.28 (1H), 7.05 (1H), 4.75 (2H), 4.57 (2H), 3.21 (3H), 2.98 (3H), 2.87 (2H), 2.61 (2H), 1.76 (2H), 1.52 (2H), 1.28–1.14 (24H), 0.8 (6H). ^{13}C NMR (400 MHz, DMSO- d_6 , δ ppm): 165.87, 165.45, 159.51, 158.05, 157.91, 156.99, 156.48, 156.42, 155.51, 153.89, 153.41, 153.04, 152.00, 151.55, 150.66, 138.99, 138.03, 137.60, 136.50, 133.55, 132.53, 130.73, 130.46, 129.35 128.46, 127.75, 127.43, 126.95, 126.58, 125.67, 124.72, 124.16, 124.00, 123.37, 123.06, 66.68, 66.47, 53.12, 52.99, 35.13, 34.73, 31.75, 31.65, 30.22, 30.07, 29.42, 29.32, 29.26, 29.17, 29.12, 29.04, 22.56, 22.50, 14.41, 14.36) (Figures S10 and S11).

2.4. Dye Sensitized Solar Cell (DSSC) Fabrication

FTO glasses were first cleaned in a 2-propanol solution by using an ultrasonic bath for 10 min. and then heated at 450 °C for 20 min. The compact TiO $_2$ blocking underlayer

was fabricated by spincoating (10 s at 1000 rpm, 2 s at 2000 rpm) a 0.3 M titanium tetraisopropoxide solution in 1-butanol, followed by drying at room temperature, and heating in air at 500 °C for 15 min. The TiO₂ colloidal paste for the porous nanocrystalline film was applied on top of the blocking layer by manually spreading the TiO₂ paste by sliding a glass blade over two strips of 3M scotch tape placed at an interdistance of 0.5 cm. The wet films were thermally treated according to the following temperature program: from RT to 120 °C at 10 °C/min, from 120 °C to 450 °C at 11 °C/min, rest at 450 °C for additional 30 min followed by ramping at 500 °C at 5 °C/min, and resting at 500 °C for 10 min. Cooling at RT occurred naturally. TiCl₄ treatment of the sintered TiO₂ films was performed by drop casting 0.4 M TiCl₄ followed by overnight hydrolysis at room temperature in a closed chamber. A final treatment at 450 °C for 30 min in air was instrumental in consolidating the TiO₂ overlayer created on top of the titania nanoparticles upon slow hydrolysis of TiCl₄. The typical thickness of the resulting film was of the order of 8 μm [20]. Sensitization was achieved by overnight immersion of transparent titania films in an appropriate staining solution of selected dye sensitizers: 0.2 mM of Z907 in ethanol; 0.19 mM of 3 in ethanol; 0.18 mM of 4 (2Z907-Ag⁺-(Ru(TMAM))) in (21:1 v:v ethanol:acetonitrile) solution.

PEDOT counter electrodes for DSSCs were prepared by multicyclic potentiodynamic electropolymerization of a 10⁻² M EDOT/0.1 M LiClO₄ acetonitrile solution with cofacially assembled electrodes held at a 2.3 mm distance. FTO was the working electrode and a platinum sheet the counter electrode. Typically, two potential cycles from 0 to 1.7 V vs. SCE at 50 mV/s afforded a homogeneous PEDOT film with a 0.25 cm² geometric active area [21].

DSSCs were prepared in an open configuration by using surlyn 25 as a spacer. The composition of the cobalt based electrolytes is as follows: 0.28 M/0.018 M Co(bpy)₃^{2+/3+}, 0.1 M LiOTf, and 0.2 M TBPY in acetonitrile.

3. Results and Discussion

3.1. Spectroscopic Properties

3.1.1. [Ru(TMAM)₂CN₂][TFSI₄] (1)

The UV-Vis spectra of 1 (RuTMAM) compared with the dichloride precursor complex [Ru(TMAM)₂Cl₂]⁴⁺ are reported in Figure 2a. Both complexes showed two broad mixed character MLCT-LLCT (Metal to Ligand Charge Transfer-Ligand to Ligand Charge Transfer) bands [22] spanning the visible range and a sharp and intense ligand centered π-π* transition at ca. 300 nm. The blue shift of ca. 40 nm of the MLCT band maxima observed upon substitution of the chloride ligands with the CN⁻ groups was consistent with the stabilization of dπ orbitals of Ru(II) due to back bonding to π* orbitals of the cyano ligands. This compound exhibits a quasi-reversible Ru(II)/Ru(III) oxidation process (ΔE = 120 mV) with E_{1/2} = 960 mV vs. SCE (Figure 2b). 1 (Ru(TMAM)) emits from the lowest triplet state (T₁) in aerated fluid solution with an E⁰⁰ evaluated from the crossing of the normalized absorption and emission spectra of 2.13 eV.

3.1.2. Multinuclear Systems

The realization of self-assembly systems via Ag⁺ bridges benefits from previous literature where (Bu₄N)₂Ru(DCBH)₂(NCS)₂ [23] (DCBH₂ = 4,4' dicarboxy-2,2' bipyridine) and the complex Ru(bpy)₂(CN)₂ [11] (bpy = 2,2' bipyridine) were able to interact with Ag⁺ by using the non-bonding σ pairs of either nitrogen or sulfur atoms of CN and NCS ligands. In particular, in the case of CN groups, high CN-Ag⁺ association constants have been reported, indicating the possibility of exploiting these building blocks to create multinuclear species of different stoichiometry.

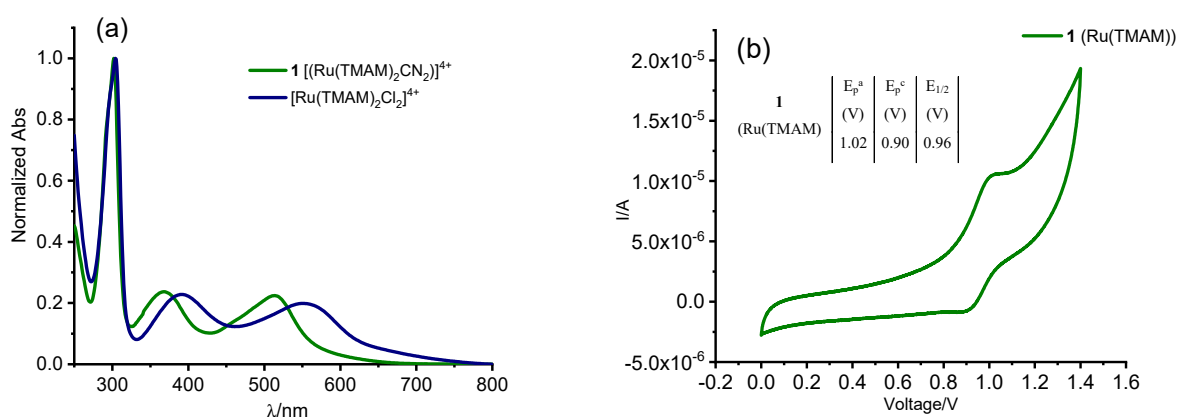


Figure 2. (a) Comparison between the normalized absorption spectra of **1** $[\text{Ru}(\text{TMAM})_2\text{CN}_2]^{4+}$ (green line) and of the precursor $[\text{Ru}(\text{TMAM})_2\text{Cl}_2]^{4+}$ (violet line) values in ethanol. (b) Cyclic voltammetry of **1** (Ru(TMAM)) in 0.1M $\text{LiClO}_4/\text{ACN}$ at 50 mV/s at a glassy carbon electrode. Voltage is referred to SCE.

As a general electronic effect, the coordination by Ag^+ causes the stabilization of $d(\pi)$ of the Ru(II), resulting in a hypsochromic shift of the MLCT transitions. When **Z907** or **1** (Ru(TMAM)) are mixed with Ag^+ in a proper stoichiometric ratio (2 **Z907**:1 Ag^+ (**3**) and **1** Ru(TMAM): 1 Ag^+ (**2**)), one observes a blue shift of the visible bands of the order of ca. 25–30 nm, associated with a ca. 20% decrease in the extinction coefficient of the charge transfer bands (Table 1 and Figure 3). This is suggestive of a decreased transition dipole consistent with the electron withdrawing effects of Ag^+ , which decreases the electron density of both Ru(II) and ancillary ligands. IR spectroscopy provides further proof of Ag^+ coordination since, upon coordination of the latter, the stretching bands of both NCS and CN split, with the appearance of a band peaking at a frequency of 30/40 cm^{-1} higher than that of the uncoordinated groups (Figure S12). This band originates from the kinematic coupling and is typical of bridging ligands (i.e., Ag-NC-Ru and Ag-SCN-Ru groups) where the motion of either NCS or CN groups is constrained by the presence of a second metal center [24,25].

Table 1. Spectroscopic features of the different systems in ethanol.

	Absorption			Emission		E^{00}/eV
	$\lambda_{\text{max}}/\text{nm}$ MLCT	$\epsilon/\text{M}^{-1}\text{cm}^{-1}$ MLCT	λ/nm $\pi-\pi^*$	$\lambda_{\text{max}}/\text{nm}$	τ^*/ns	
Z907	540, 417	12,047, 12,935	315, 295 ^{Sh}	>850	<10	1.71
1 (Ru(TMAM))	490, 358	10,858, 9487	301	700	189	2.13
2 (Ru(TMAM)- Ag^+)	467, 343	9520, 9498	299	665	222	2.18
3 (2 Z907 - Ag^+)	514, 406	9011, 9384	314, 295 ^{Sh}	790	23	2.03
4 (2 Z907 - Ag^+ - Ru(TMAM))	503, 442 ^{Sh} , 361	13,570, 12,944	314 ^{Sh} , 300	744	/	/

Sh = shoulder, * = methanol.

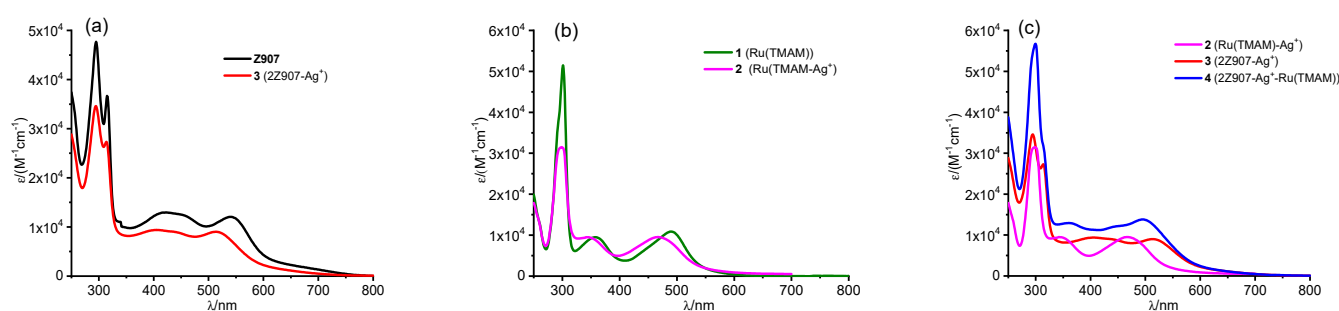


Figure 3. Comparison between absorption spectra of: (a) **Z907** (black line) and **3** (**2Z907-Ag⁺**) (red line), (b) **1** (**Ru(TMAM)**) (green line) and **2** (**Ru(TMAM)-Ag⁺**) (purple line) and (c) between **2** (purple line), **3** (red line) and **4** (**2Z907-Ag⁺-Ru(TMAM)**) (blue line).

4 (**2Z907-Ag⁺-Ru(TMAM)**) exhibits UV-Vis spectral features that are the exact sum of the individual complexes **3** and **2** (Figure 3 and Figure S13). This results in a wide visible absorption in the visible region, up to 700 nm, with an average extinction coefficient of ca. $1.4 \times 10^4 \text{ M}^{-1} \text{ cm}^{-1}$ between 500 and 350 nm. The IR signature of the NCS and CN groups bridged by Ag^+ is also the result of the individual contribution of the composing fragments **2** (**Ru(TMAM)-Ag⁺**) and **3** (**2Z907-Ag⁺**), corroborating the identity and the proposed stoichiometry of such compound. The complex **2** (**Ru(TMAM)-Ag⁺**) emits in ethanolic solution due to radiative deactivation of the lowest triplet state (T_1) with an E^0 of 2.18 eV and a monoexponential lifetime of 222 ns, which was increased with respect to the parent compound **1** (**Ru(TMAM)**) (189 ns). The increased emission lifetime is consistent with the energy gap law [26,27]. The complex **3** (**2Z907-Ag⁺**) also showed an increased spectroscopic energy (E^0 2.03 eV) with respect to the parent **Z907** compound (1.71 eV) and an increased emission lifetime of 23 ns with respect to less than 10 ns for the latter (Table 1). The 450 nm excitation of an isoabsorbing (with the respect to **2** (**Ru(TMAM)-Ag⁺**)) solution of compound **4** (**2Z907-Ag⁺-Ru(TMAM)**) revealed a considerable, but incomplete quenching of the emission centered on the Ru(TMAM) antenna due to energy transfer to the Z907 units. The incomplete quenching is evidenced by the broad emission band (Figure 4a, blue line) of the complex **4** (**2Z907-Ag⁺-Ru(TMAM)**), which bears both the contribution from the fragments **3** (**2Z907-Ag⁺**) and **2** (**Ru(TMAM)-Ag⁺**), resulting in an emission maximum (ca. 720 nm) which is an intermediate between that of **3** (**2Z907-Ag⁺**) (790 nm) (Figure 4a, red line) and that of **2** (**Ru(TMAM)-Ag⁺**) (665 nm) (Figure 4a, purple line). We have, however, observed partial photodissociation of complex **4** upon 450 nm excitation, which also resulted in the formation of a silver colloid in solution. In order to stabilize **4** (**2Z907-Ag⁺-Ru(TMAM)**), we resorted to its immobilization on a ZrO_2 thin film, which is an inert semiconductor whose conduction band is not energetically accessible to the oxidative quenching of the excited state by electron transfer [28–30]. Actually, partial injection dynamics in sub-band gap states of ZrO_2 have been reported in the case of strongly reducing excited states of organic chromophores [31,32]. However, the excited state oxidation potential of those species was from ca. -400 to -600 meV higher than the Ru(II) species investigated in this work, from which we can thus expect a very marginal quenching by injection on zirconia substrates. When **4** was loaded on ZrO_2 , we observed that no residual emission of fragment **2** (**Ru(TMAM)-Ag⁺**) was present in the emission spectrum of species **4** (Figure 4b, blue line), whose emissive features coincided with those of fragment **3** (**2Z907-Ag⁺**) (Figure 4b, red line). This confirms that the energy funneling from the antenna to the injecting units is, within the sensitivity of this technique, complete. We note that the improved stability of **4**, once adsorbed on semiconductor thin films can be explained by the lack of translational degrees of freedom of the coordinated metal fragments, which, being blocked together by the interaction with the surface can re-associate after a possible photodissociation event. On the other hand, in solution, dissociated fragments can diffuse away before re-association can occur, resulting

in the irreversible photochemical reduction of Ag^+ , which leads to the formation of the observed silver colloids.

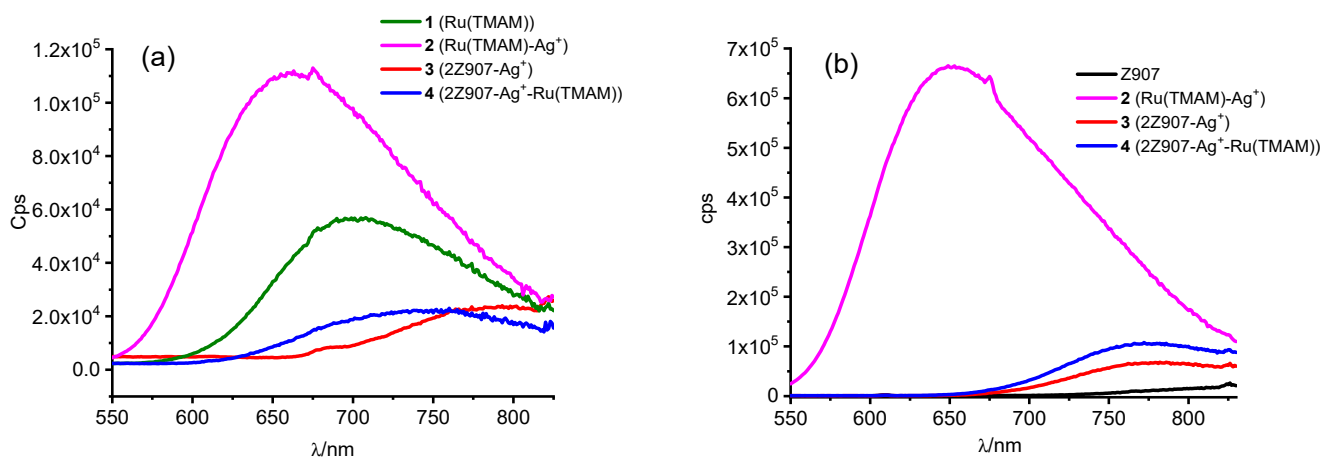


Figure 4. Emission spectra ($\lambda_{\text{exc}} = 450 \text{ nm}$) of (a) **1** Ru(TMAM) (green line), **2** (Ru(TMAM)-Ag⁺) (purple line), **3** (2Z907-Ag⁺) (red line), and **4** (2Z907-Ag⁺-Ru(TMAM)) (blue line) in ethanolic solutions and of (b) **Z907** (black line), **2** (Ru(TMAM)-Ag⁺) (purple line), **3** (2Z907-Ag⁺) (red line), and **4** (2Z907-Ag⁺-Ru(TMAM)) (blue line) supported on ZrO₂.

3.2. Time Resolved Spectroscopy in Solution and on ZrO₂ Thin Films

The 532 nm laser excitation (FWHM of 7 ns) of the coordination compounds herein reported led to the population of the lowest triplet charge transfer state within the instrumental time response (Figure 5). We note that excitation was in the CT absorption manifold of both the **1** (Ru(TMAM)) and **Z907** related moieties. Species **3** (2Z907-Ag⁺) exhibited transient spectroscopic features that are summarized by the bleaching of the ground state absorption bands at 450 and 540 nm, followed by a broad triplet absorption with a maximum at ca. 680 nm. A weak negative band followed in the NIR region caused by spontaneous emission, consistent with the previously discussed steady state emissive properties. **1** (Ru(TMAM)) and **2** (Ru(TMAM)-Ag⁺) displayed nearly identical triplet features with an intense ground state bleaching at ca. 490 nm followed by the spontaneous emission in the 600–800 nm interval. A high energy absorption rose for $\lambda < 430 \text{ nm}$. The transient spectrum of the **4** (2Z907-Ag⁺-Ru(TMAM)) compound was almost identical to that of the **2** (Ru(TMAM)-Ag⁺) since, at the same laser excitation energy, **2** featured ΔA amplitudes that were about ten times larger (up to $-500 \text{ m}\Delta\text{OD}$ vs. $-60 \text{ m}\Delta\text{OD}$) than those of the **Z907** fragment. In addition, the residual spontaneous emission of photodissociated **1** (Ru(TMAM)) or **2** (Ru(TMAM)-Ag⁺) fragments, resulting in a bleaching band at $\lambda > 650 \text{ nm}$, offset the much weaker absorption of the excited state centered on the **Z907** units. This corroborates the indication of limited photostability of the tetranuclear adduct **4** in solution under visible light excitation.

For the complexes under investigation, the absorption and scattering properties of the ZrO₂ thin films prevented a fruitful application of the time resolved absorption spectroscopy, however, the emission properties could be studied with some detail. The transient emission spectra, taken on sensitized ZrO₂, revealed the distinct emission features of the complexes **2** (Ru(TMAM)-Ag⁺) (Figure 6a) and **3** (2Z907-Ag⁺) (Figure 6b). For the former, the emission maximum was found at 640 nm, with an average lifetime of 41 ns. The shortening of the excited state lifetime, with respect to the solution kinetics, was due to aggregation of the chromophores on the semiconductor surface, which enhanced the non-radiative deactivation pathways of the triplet state, whereas the multiexponential decay stemmed from the heterogeneity of surface adsorption sites, which caused a dispersion in excited state energetics and a distribution in decay rates. Compound **3** (2Z907-Ag⁺) exhibited an emission centered at 750 nm, substantially convolved with the time response of the laser pulse. Sampling of the emission signal allowed us to well define the shape of the band

up to a delay of 26 ns after the laser pulse. The shape of emission spectrum of complex **4** ($2Z907\text{-Ag}^+\text{-(Ru(TMAM))}$), Figure 6c, was nearly identical to that of species **3** (2907-Ag^+), except for a very small shoulder observed around 640 nm and assigned to a residual unquenched **2** (Ru(TMAM)-Ag^+) emission. This residual intensity, upon normalization by the light harvesting of the film at the excitation wavelength, provided a quenching efficiency of 94%. The analysis of the 640 nm emission decay by TCSPC (Figure S14) showed a substantial reduction of the lifetime with respect to **2** (Ru(TMAM)-Ag^+) alone. The decay kinetics exhibited a two component decay of which the largely dominant one was below the instrumental time resolution of our apparatus (300–500 ps), also suggestive of an energy transfer process that occurs with an efficiency of 99%, in good agreement with the estimate made on the basis of the emission intensity.

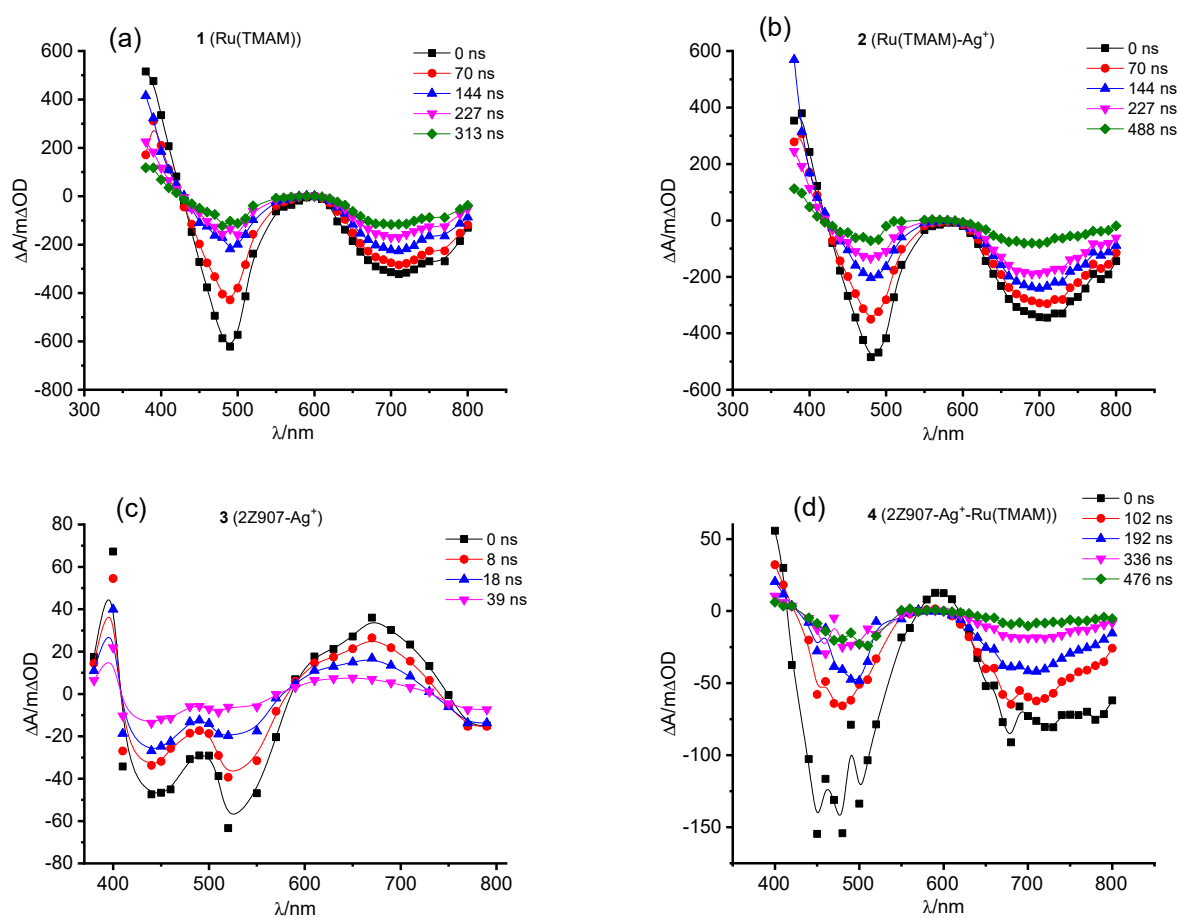


Figure 5. Transient absorption spectra (TAS) of (a) **1** Ru(TMAM) (b) **2** (Ru(TMAM)-Ag⁺), (c) **3** (2907-Ag⁺), and (d) **4** (2Z907-Ag⁺-(Ru(TMAM))) recorded in methanol upon 532 nm laser excitation.

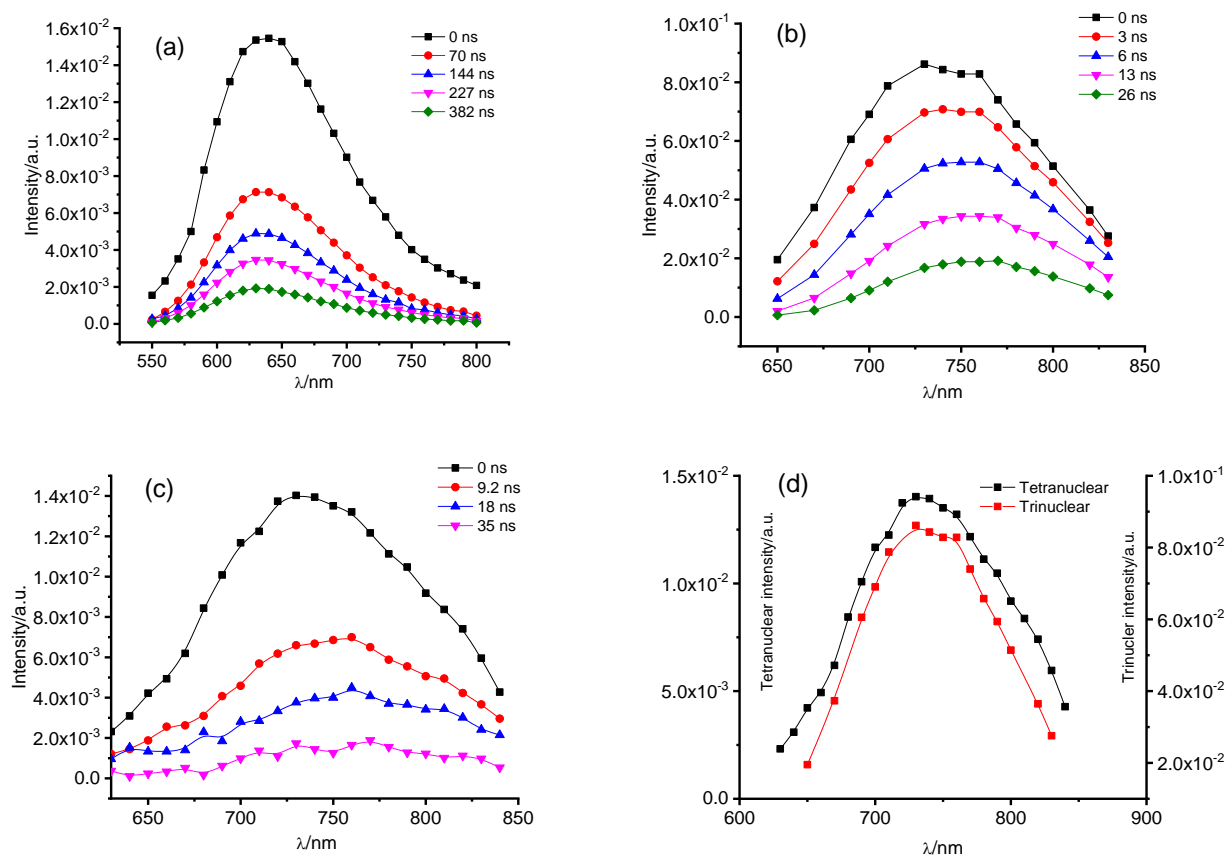


Figure 6. Time resolved emission profiles on ZrO_2 thin film: (a) **2** ($Ru(TMAM)-Ag^+$), (b) **3** ($Z907-Ag^+$), (c) **4** ($2Z907-Ag^+-Ru(TMAM)$), and (d) Comparison between emission spectra of complex **3** and of complex **4** at 0 delay. Thin films are in contact with 0.1 M Li^+ in ACN.

3.3. TiO_2 Sensitization

Both the adducts **3** and **4** incorporating **Z907** complexes adsorb spontaneously on TiO_2 . The adsorption of **1** ($Ru(TMAM)$) and of its binuclear derivative **2** ($Ru(TMAM)-Ag^+$) is quite weak, and occurs by a mixture of electrostatic interactions or via acid–base interaction of the CN lone pair with $Ti(IV)$. While this interaction is sufficiently strong to allow some spectroscopic studies, like the ZrO_2 emission discussed before, it is far too weak to guarantee a sizable light harvesting for energy conversion application. We thus focused mainly on the behavior of the **Z907** containing multinuclear complexes. Absorption spectra of the sensitized titania films are reported in Figure 7a, showing that both complexes **4** and **3** exhibited a very strong spectral similarity in the visible region. With respect to **Z907** alone, a blue shifted absorption was obtained, with a main visible band peaking at 525 nm, with an optical density ca. 40% higher than the **Z907** sensitized thin film. A further confirmation of the assigned nuclearity of the complexes loaded on the TiO_2 film can be gained by cyclic voltammetry, where, given the insulating nature of TiO_2 at anodic potentials, one relies on the oxidation of species electronically coupled with the FTO collector and subsequent charge hopping between adjacent surface adsorbed species. Through cyclic voltammetry (Figure S15), we observed that in species **3** ($2Z907-Ag^+$), the intensity of the anodic wave associated to the $Ru(II)/(III)$ oxidation in **Z907** (ca. 0.7 V vs. SCE) was positively shifted (by ca. 100 mV) and nearly doubled in intensity, given that the 2 **Z907** units bridged by Ag^+ , being weakly coupled, underwent simultaneous oxidation. In compound **4** ($2Z907-Ag^+-(Ru(TMAM))$), the bielectronic anodic wave corresponding to the oxidation of the 2 **Z907** fragments was accompanied by a second more positive wave at ca. 1.1 V vs. SCE, having ca. half intensity with respect to the former and is

consistent, by comparison with the redox behavior of the mononuclear analog in solution, with the Ru(II)/Ru(III) oxidation localized on the unit **1** (Ru(TMAM)). The surface loading, computed from $A(\lambda) = 1000\Gamma\epsilon(\lambda)$ was for the significant cases (**Z907** containing species) of the order of 10^{-7} mol/cm² (Figure 7b), with the highest chromophore concentration found for species **3** (2Z907-Ag⁺) (1.5×10^{-7} mol/cm²), which nearly completely offset the intrinsically superior light harvesting properties of **4** (2Z907-Ag⁺-Ru(TMAM)), which achieved a 33% lower concentration, probably due to a combination of higher steric hindrance and electrostatic repulsion between the adsorbed species. The 532 nm excitation of **3** (2Z907-Ag⁺) and of **4** (2Z907-Ag⁺-Ru(TMAM)) resulted in both cases, within the instrumental time resolution of our spectrometer (10 KOhm pre-amplifier), in the generation of a very long lived charge separated state corresponding to Z907⁺/e⁻ (TiO₂) (Figure 8). Such a charge separated state does not recover on a time scale of 1 ms (Figure S16), leaving plenty of time for regeneration from the redox electrolyte to occur. It should be noted that, since the oxidation of the unit **1** (Ru(TMAM)) is more positive than that of **Z907**, the hole remains confined within such a unit. The transient spectrum of the charge separated state in **3** (2Z907-Ag⁺) (Figure 8a) showed the bleach of the ground state absorption localized on the **Z907** fragment followed by a structured absorption in the red region, with a shoulder at 600 nm and a more intense band centered around 800 nm due to mixed contributions of LMCT transitions and TiO₂ trapped electron absorption [20]. This low energy spectral fingerprint was also found in compound **4** (2Z907-Ag⁺-Ru(TMAM)) (Figure 8b), where the absence of residual emission from the Ag⁺ bridged fragment **1** (Ru(TMAM)) was consistent with the nearly complete energy transfer from this antenna to the **Z907** moieties, which then deactivate by electron injection on a sub-ns time scale.

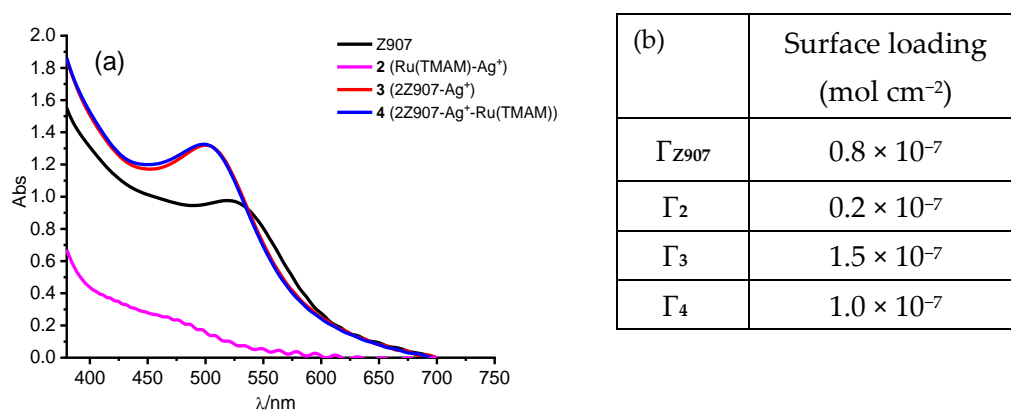


Figure 7. (a) Absorption spectra on TiO₂ for **Z907** (black line), **2** (Ru(TMAM)-Ag⁺) (purple line), **3** (2Z907-Ag⁺) (red line), and **4** (2Z907-Ag⁺-Ru(TMAM)) (blue line). (b) Dyes loading onto TiO₂ calculated with the ϵ data reported in Table 1.

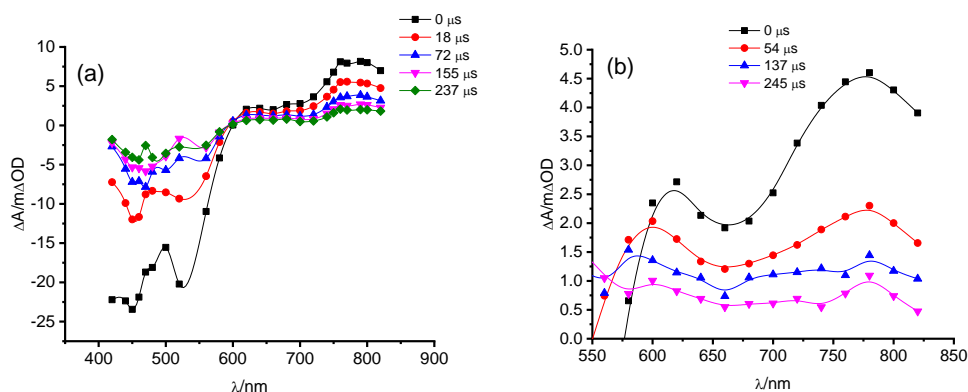


Figure 8. TAS recorded on TiO₂ for (a) **3** (2Z907-Ag⁺) and for (b) **4** (2Z907-Ag⁺-Ru(TMAM)). Thin films are in contact with 0.1 M Li⁺ in CAN.

3.4. Photo-Electrochemical Characterization

Figure 9a reports the photoaction spectra (IPCE vs. λ) of complexes **3** and **4** compared to **Z907**. The maximum photoconversion in the presence of the $[\text{Co}(\text{bpy})_3]^{2+/3+}$ couples is of the order of 65/70% and is achieved by complex **4**, which significantly outperformed the **Z907** (ca. 50% maximum conversion). Complex **4** was also slightly superior to **3**. The IPCE is the product of three terms according to $\text{IPCE} = \Phi_{\text{inj}} \times \eta_{\text{coll}} \times \text{LHE}$. Since injection occurs from the **Z907** units based on our and on other evidence [33], the injection efficiency Φ_{inj} can be considered close to unity. The LHE (calculating according to $\text{LHE} = 1 - 10^{-A(\lambda_{\text{max}})}$) was 90% for **Z907** and 95% for the other two cases, hence the observed 20% conversion difference was mostly related to an improved η_{coll} when the multinuclear species were used. This effect may arise from a slight acceleration in Ru(II) regeneration, following the ca. 100 meV increase in the driving force for Co(II) oxidation, but most importantly from a substantial reduction in the dark current (Figure 9b dashed line) due to a combination of steric and electrostatic shielding in the presence of **3** and **4**. This result is motivated by a combination of electrostatic repulsion and steric shielding of the TiO_2 surface, which is protected by a higher density of long alkyl chains and quaternary ammonium ions, which contribute to repel positively charged Co(III) ions present in the electrolyte.

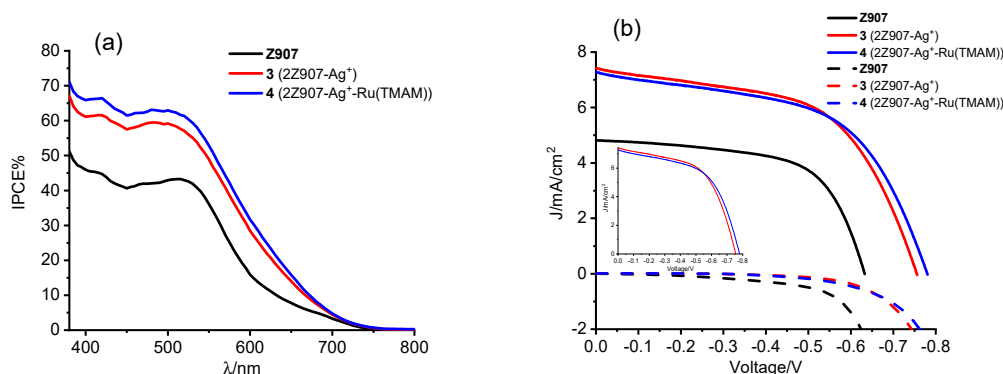


Figure 9. (a) IPCE spectra and (b) JV curves for **Z907** (black line), **3** (2Z907-Ag^+) (red line) and **4** ($2\text{Z907-Ag}^+\text{-Ru(TMAM)}$) (blue line) recorded under 0.1 W/cm^2 AM 1.5 G illumination.

As a result, the efficiency of transparent cells increased from 1.9% (**Z907**) to 3.1% when **3** and **4** were used (Table 2 and Figure 9b). The J_{sc} of the cells agreed with the integrated photocurrent spectrum recorded during IPCE measurement (Figure S17). Actually, the integrated photocurrent was slightly higher than that observed under white light, where the cell probably suffers from partial diffusional limitations arising from the use of Co(II)/(III) electron mediators in association with a TiO_2 film made of small 18–20 nm particles. Indeed, the best conversion efficiency with redox mediators based on coordination compounds were reported with 30 nm particles, which created a sintered titania film with larger voids and channels for the unimpeded diffusion of bulky electron mediators [4].

Table 2. Photovoltaic parameters of **Z907**, **3** (2Z907-Ag^+), and **4** ($2\text{Z907-Ag}^+\text{-Ru(TMAM)}$) sensitized cells recorded in the presence of $[\text{Co}(\text{bpy})_3]^{2+/3+}$ redox mediator. The efficiency parameters were obtained by averaging the performance of a set of 5 cells.

	$J/\text{mA/cm}^2$	V_{oc}/V	FF%	η %
Z907	4.8 ± 0.2	0.64 ± 0.08	62 ± 3	1.9 ± 0.2
3 (2Z907-Ag^+)	7.4 ± 0.4	0.75 ± 0.02	56 ± 4	3.1 ± 0.1
4 ($2\text{Z907-Ag}^+\text{-Ru(TMAM)}$)	7.3 ± 0.2	0.78 ± 0.01	55 ± 1	3.1 ± 0.1

The electron lifetime τ_{el} obtained from the open circuit photovoltage decay (Figure 10a) according to Bisquert et al. [34] confirmed the superior screening achieved with the multinuclear complexes **3** and **4** (Figure 10a, red and blue symbols), with respect to **Z907** alone (black). In particular, **4** spanned the longest lifetime of the series (i.e., >0.1 s) within a photopotential range comprised between -0.2 V and -0.5 V. At the maximum photopotential (ca. -0.8 V), the electron lifetime of **3** and **4** achieved similar values (10–13 ms) and was longer than that of **Z907** by a ca. $3\times$ factor, consistent with the control experiments by EIS, where the $-Z''$ vs. frequency plot (Figure 10b) originated by the sensitized TiO_2 /electrolyte interface led to an entirely analogous trend.

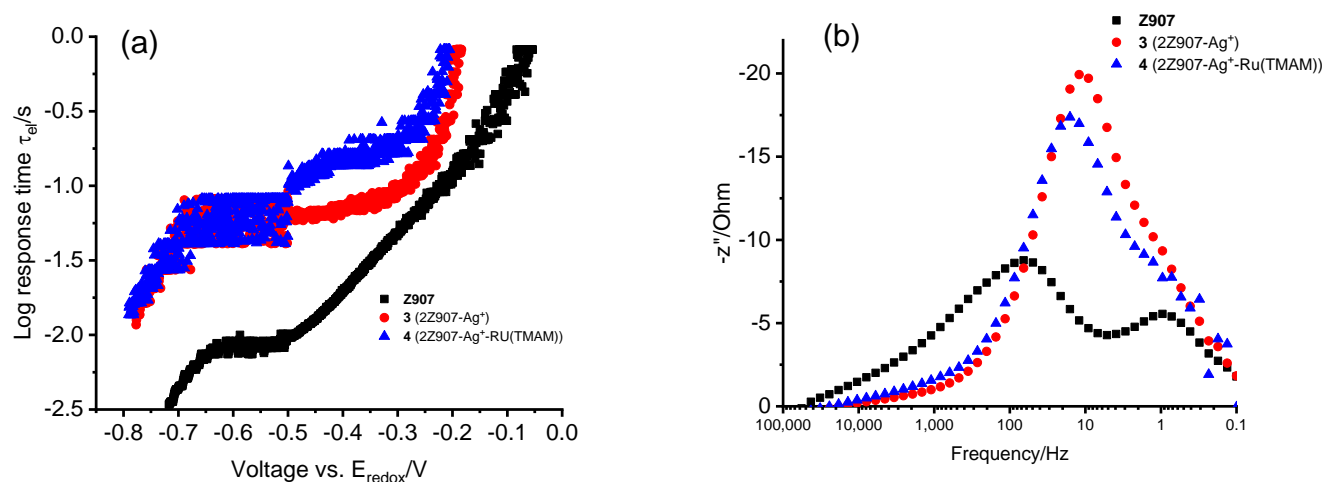


Figure 10. (a) Open circuit photovoltage decay of **Z907** (black), **3** (red), and **4** (blue) sensitized solar cells; (b) $-Z''$ vs. frequency plot of the same cells held at open circuit voltage.

4. Conclusions

A multinuclear compound **4** comprising a $\text{Ru(TMAM)}_2(\text{CN}_2)]^{4+}$ (TMAM = (bis-4,4'-bis(trimethylaminomethyl)2,2'-bipyridine) and 2 **Z907** units was obtained by bridging the ancillary ligands with Ag^+ ions. **4** displayed antenna effect revealing >95% energy transfer from the Ru(TMAM) unit to the **Z907** species interacting with the titania surface (Figure 11). As a result, a $0.1 \mu\text{M}/\text{cm}^2$ surface concentration of **4** allows for a 95% harvesting efficiency of green photons, which are converted to electrons with an external quantum yield of ca. 65–70%. Compared to **Z907**, the efficiency of the multinuclear adduct in a transparent DSSC was approximately doubled, however, the improvement, with respect to the multinuclear assembly (**3**) encompassing 2 **Z907** complexes bridged by Ag^+ , was quite marginal because of the 50% higher surface concentration achieved by the latter. This led to nearly identical harvesting efficiency within the same spectra region. When a fast redox couple like the $[\text{Co}(\text{bpy})_3]^{3+/2+}$ uses a multinuclear assembly, it provides the possibility of obtaining a superior shielding with respect to the parent mononuclear compound, which brings to a substantial reduction of the recombination current arising from electron recapture by Co(III) species. This shielding was achieved by both steric and electrostatic effects.

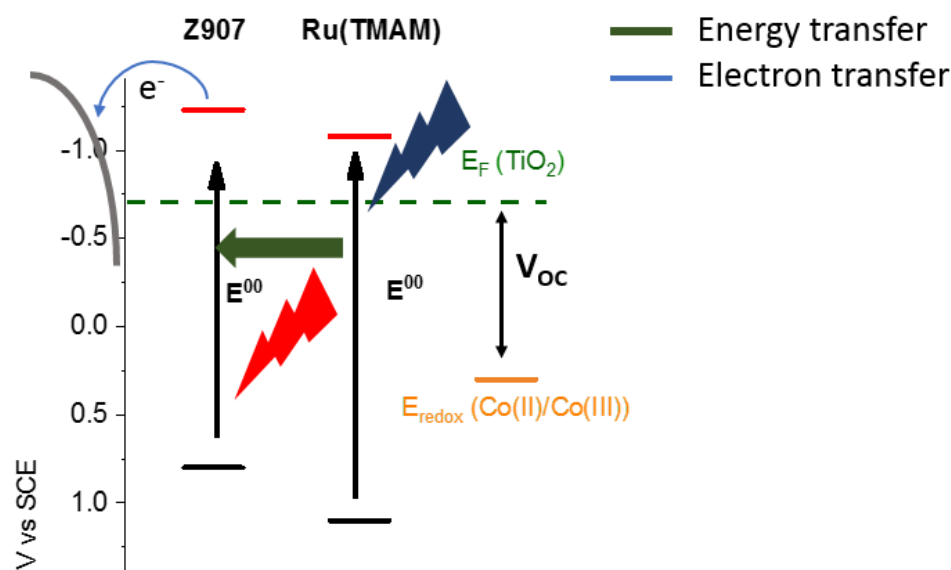


Figure 11. Energy level diagram involving the ground and the lowest excited states of **4** and the resulting energy and electron transfer pathways. Absorption of higher energy photons is realized by the RuTMAM unit that funnels energy to Z907, which undergoes photoinduced injection.

Supplementary Materials: The following are available online at <https://www.mdpi.com/2076-3417/11/6/2769/s1>, Figure S1: Structure of the synthe-sized species, Figure S2: ^1H -NMR spectrum of the TMAM ligand, Figures S3 and S4: ^1H and ^{13}C NMR spectra of the complex 1 (Ru(TMAM)), Figure S5: SI-MS spectrum of the complex 1 (Ru(TMAM)), Figures S6 and S7: ^1H and ^{13}C NMR spectra of the complex 2 ((Ru(TMAM))- Ag^+), Figures S8 and S9: ^1H and ^{13}C NMR spectra of the complex 3 (Z907- Ag^+), Figure S10: ^1H NMR (400 MHz, DMSO- d_6 , δ ppm) of the complex 4 (Z907- Ag^+ -Ru(TMAM)), Figure S11: ^{13}C NMR (400 MHz, DMSO- d_6 , δ ppm) of the complex 4 (Z907- Ag^+ -Ru(TMAM)), Figure S12: Spectroscopic features of the complexes, Figure S13: Comparison between calculated and experimental absorption spectra of the complex 4 (Z907- Ag^+ -Ru(TMAM)), Figure S14: TCSPC decay on ZrO_2 , Figure S15: Cyclic voltammetry of the complexes loaded on TiO_2 , Figure S16: Charge separated state decay of 3 (Z907- Ag^+), Figure S17: Integrated current density.

Author Contributions: Conceptualization, C.A.B. and S.C.; Methodology, R.B., C.A.B. and S.C.; Investigation, E.M., R.B., V.C., R.A. and A.N.; Resources, S.C.; Data curation, E.M., V.C. and R.A.; Writing—Original draft preparation E.M. and C.A.B.; Writing—Review and editing, S.C. and E.M. All authors have read and agreed to the published version of the manuscript.

Funding: E.M. thanks the Fondo Sociale Europeo, regione Emilia Romagna for a grant.

Institutional Review Board Statement: Not applicable.

Informed Consent Statement: Not applicable.

Data Availability Statement: Not applicable.

Acknowledgments: We gratefully thank F.N. Castellano (N.C. State University) and G.J. Meyer (UNC) for their fruitful discussions and the generous loan of 4-4'-bis(bromomethyl)-2-2'-bipyridine.

Conflicts of Interest: The authors declare no conflict of interest.

References

- O'Regan, B.; Grätzel, M. A low-cost, high-efficiency solar cell based on dye-sensitized colloidal TiO_2 films. *Nature* **1991**, *353*, 737–740. [[CrossRef](#)]
- Hagfeldt, A.; Boschloo, G.; Sun, L.; Kloo, L.; Pettersson, H. Dye-sensitized solar cells. *Chem. Rev.* **2010**, *110*, 6595–6663. [[CrossRef](#)] [[PubMed](#)]
- Cornaro, C.; Renzi, L.; Pierro, M.; Di Carlo, A.; Guglielmotti, A. Thermal and Electrical Characterization of a Semi-Transparent Dye-Sensitized Photovoltaic Module under Real Operating Conditions. *Energies* **2018**, *11*, 155. [[CrossRef](#)]

4. Tanaka, E.; Michaels, H.; Freitag, M.; Robertson, N. Synergy of co-sensitizers in a copper bipyridyl redox system for efficient and cost-effective dye-sensitized solar cells in solar and ambient light. *J. Mater. Chem. A* **2020**, *8*, 1279–1287. [[CrossRef](#)]
5. Kakiage, K.; Aoyama, Y.; Yano, T.; Oya, K.; Fujisawa, J.; Hanaya, M. Highly-efficient dye-sensitized solar cells with collaborative sensitization by silyl-anchor and carboxy-anchor dyes. *Chem. Commun.* **2015**, *51*, 15894–15897. [[CrossRef](#)] [[PubMed](#)]
6. Saygili, Y.; Soderberg, M.; Pellet, N.; Giordano, F.; Cao, Y.; Munoz-Garcia, A.B.; Zakeeruddin, S.M.; Vlachopoulos, N.; Pavone, M.; Boschloo, G.; et al. Copper Bipyridyl Redox Mediators for Dye-Sensitized Solar Cells with High Photovoltage. *J. Am. Chem. Soc.* **2016**, *138*, 15087–15096. [[CrossRef](#)]
7. Hagberg, D.P.; Jiang, X.; Gabrielson, E.; Linder, M.; Marinado, T.; Brinck, T.; Hagfeldt, A.; Sun, L.C. Symmetric and unsymmetric donor functionalization. comparing structural and spectral benefits of chromophores for dye-sensitized solar cells. *J. Mater. Chem.* **2009**, *19*, 7232–7238. [[CrossRef](#)]
8. Tsao, H.N.; Yi, C.; Moehl, T.; Yum, J.H.; Zakeeruddin, S.M.; Nazeeruddin, M.K.; Gratzel, M. Cyclopentadithiophene bridged donor-acceptor dyes achieve high power conversion efficiencies in dye-sensitized solar cells based on the tris-cobalt bipyridine redox couple. *ChemSusChem* **2011**, *4*, 591–594. [[CrossRef](#)] [[PubMed](#)]
9. Carli, S.; Casarin, L.; Caramori, S.; Boaretto, R.; Busatto, E.; Argazzi, R.; Bignozzi, C.A. A viable surface passivation approach to improve efficiency in cobalt based dye sensitized solar cells. *Polyhedron* **2014**, *82*, 173–180. [[CrossRef](#)]
10. Pradhan, A.; Kiran, M.S.; Kapil, G.; Hayase, S.; Pandey, S.S. Wide wavelength photon harvesting in dye-sensitized solar cells utilizing cobalt complex redox electrolyte: Implication of surface passivation. *Sol. Energy Mat. Sol. C* **2019**, *195*, 122–133. [[CrossRef](#)]
11. Kinnaird, M.G.; Whitten, D.G. Luminescent bimetallic complexes. Study of the formation, redox behavior, and photochemistry of complexes between Ag⁺ and bis(2,2'-bipyridine)-bis-cyanoruthenium(II). *Chem. Phys. Lett.* **1982**, *88*, 275–280. [[CrossRef](#)]
12. Amadelli, R.; Argazzi, R.; Bignozzi, C.A.; Scandola, F. Design of Antenna-Sensitizer Polynuclear Complexes—Sensitization of Titanium-Dioxide with [Ru(Bpy)₂(Cn)₂]₂ru(Bpy(Coo)₂)₂-. *J. Am. Chem. Soc.* **1990**, *112*, 7099–7103. [[CrossRef](#)]
13. Casarin, L.; Swords, W.B.; Caramori, S.; Bignozzi, C.A.; Meyer, G.J. Rapid Static Sensitizer Regeneration Enabled by Ion Pairing. *Inorg. Chem.* **2017**, *56*, 7324–7327. [[CrossRef](#)] [[PubMed](#)]
14. Swords, W.B.; Li, G.; Meyer, G.J. Iodide Ion Pairing with Highly Charged Ruthenium Polypyridyl Cations in CH₃CN. *Inorg. Chem.* **2015**, *54*, 4512–4519. [[CrossRef](#)]
15. Li, J.-H.; Wang, J.-T.; Hu, P.; Zhang, L.-Y.; Chen, Z.-N.; Mao, Z.-W.; Ji, L.-N. Synthesis, structure and nuclease activity of copper complexes of disubstituted 2,2'-bipyridine ligands bearing ammonium groups. *Polyhedron* **2008**, *27*, 1898–1904. [[CrossRef](#)]
16. Cazzanti, S.; Caramori, S.; Argazzi, R.; Elliott, C.M.; Bignozzi, C.A. Efficient non-corrosive electron-transfer mediator mixtures for dye-sensitized solar cells. *J. Am. Chem. Soc.* **2006**, *128*, 9996–9997. [[CrossRef](#)]
17. Boaretto, R.; Busatto, E.; Carli, S.; Fracasso, S. Process for the Synthesis of Precursor Complexes of Titanium Dioxide Sensitization Dyes Based on Ruthenium Polypyridine Complexes. U.S. Patent Application 13/908,305, 13 February 2011.
18. Di Carlo, G.; Caramori, S.; Trifiletti, V.; Giannuzzi, R.; De Marco, L.; Pizzotti, M.; Orbelli Biroli, A.; Tessore, F.; Argazzi, R.; Bignozzi, C.A. Influence of porphyrinic structure on electron transfer processes at the electrolyte/dye/TiO₂ interface in PSSCs: A comparison between meso push-pull and beta-pyrrolic architectures. *ACS Appl. Mater. Interfaces* **2014**, *6*, 15841–15852. [[CrossRef](#)]
19. Reddy Marri, A.; Marchini, E.; Cabanes, V.D.; Argazzi, R.; Pastore, M.; Caramori, S.; Gros, P.C. Record power conversion efficiencies for iron(ii)-NHC-sensitized DSSCs from rational molecular engineering and electrolyte optimization. *J. Mater. Chem. A* **2021**. [[CrossRef](#)]
20. Mazzanti, M.; Caramori, S.; Fogagnolo, M.; Cristino, V.; Molinari, A. Turning Waste into Useful Products by Photocatalysis with Nanocrystalline TiO₂ Thin Films: Reductive Cleavage of Azo Bond in the Presence of Aqueous Formate. *Nanomaterials* **2020**, *10*, 2147. [[CrossRef](#)] [[PubMed](#)]
21. Carli, S.; Busatto, E.; Caramori, S.; Boaretto, R.; Argazzi, R.; Timpson, C.J.; Bignozzi, C.A. Comparative Evaluation of Catalytic Counter Electrodes for Co(III)/(II) Electron Shuttles in Regenerative Photoelectrochemical Cells. *J. Phys. Chem. C* **2013**, *117*, 5142–5153. [[CrossRef](#)]
22. Fantacci, S.; De Angelis, F. A computational approach to the electronic and optical properties of Ru(II) and Ir(III) polypyridyl complexes: Applications to DSC, OLED and NLO. *Coord. Chem. Rev.* **2011**, *255*, 2704–2726. [[CrossRef](#)]
23. Krüger, J.; Plass, R.; Grätzel, M.; Matthieu, H.-J. Improvement of the photovoltaic performance of solid-state dye-sensitized device by silver complexation of the sensitizer cis-bis(4,4'-dicarboxy-2,2'-bipyridine)-bis(isothiocyanato) ruthenium(II). *Appl. Phys. Lett.* **2002**, *81*, 367–369. [[CrossRef](#)]
24. Bignozzi, C.A.; Argazzi, R.; Schoonover, J.R.; Gordon, K.C.; Dyer, R.B.; Scandola, F. Electronic Coupling in Cyano-Bridged Ruthenium Polypyridine Complexes and Role of Electronic Effects on Cyanide Stretching Frequencies. *Inorg. Chem.* **1992**, *31*, 5260–5267. [[CrossRef](#)]
25. Dows, D.A.; Haim, A.; Wilmarth, W.K. Infra-red spectroscopic detection of bridging cyanide groups. *J. Inorg. Nucl. Chem.* **1961**, *21*, 33–37. [[CrossRef](#)]
26. Caspar, J.V.; Meyer, T.J. Application of the energy gap law to nonradiative, excited-state decay. *J. Phys. Chem.* **1983**, *87*, 952–957. [[CrossRef](#)]
27. Englman, R.; Jortner, J. The energy gap law for radiationless transitions in large molecules. *Mol. Phys.* **1970**, *18*, 145–164. [[CrossRef](#)]

28. Tachibana, Y.; Moser, J.E.; Gratzel, M.; Klug, D.R.; Durrant, J.R. Subpicosecond interfacial charge separation in dye-sensitized nanocrystalline titanium dioxide films. *J. Phys. Chem.* **1996**, *100*, 20056–20062. [[CrossRef](#)]
29. Santos, T.D.; Morandeira, A.; Koops, S.; Mozer, A.J.; Tsekouras, G.; Dong, Y.; Wagner, P.; Wallace, G.; Earles, J.C.; Gordon, K.C.; et al. Injection Limitations in a Series of Porphyrin Dye-Sensitized Solar Cells. *J. Phys. Chem. C* **2010**, *114*, 3276–3279. [[CrossRef](#)]
30. Koops, S.E.; O'Regan, B.C.; Barnes, P.R.; Durrant, J.R. Parameters influencing the efficiency of electron injection in dye-sensitized solar cells. *J. Am. Chem. Soc.* **2009**, *131*, 4808–4818. [[CrossRef](#)]
31. Oum, K.; Lohse, P.W.; Flender, O.; Klein, J.R.; Scholz, M.; Lenzer, T.; Du, J.; Oekermann, T. Ultrafast dynamics of the indoline dye D149 on electrodeposited ZnO and sintered ZrO₂ and TiO₂ thin films. *Phys. Chem. Chem. Phys.* **2012**, *14*, 15429–15437. [[CrossRef](#)] [[PubMed](#)]
32. Oum, K.; Flender, O.; Lohse, P.W.; Scholz, M.; Hagfeldt, A.; Boschloo, G.; Lenzer, T. Electron and hole transfer dynamics of a triarylamine-based dye with peripheral hole acceptors on TiO₂ in the absence and presence of solvent. *Phys. Chem. Chem. Phys.* **2014**, *16*, 8019–8029. [[CrossRef](#)] [[PubMed](#)]
33. Tiwana, P.; Docampo, P.; Johnston, M.B.; Snaith, H.J.; Herz, L.M. Electron mobility and injection dynamics in mesoporous ZnO, SnO₂, and TiO₂ films used in dye-sensitized solar cells. *ACS Nano* **2011**, *5*, 5158–5166. [[CrossRef](#)] [[PubMed](#)]
34. Bisquert, J.; Zaban, A.; Greenshtein, M.; Mora-Sero, I. Determination of rate constants for charge transfer and the distribution of semiconductor and electrolyte electronic energy levels in dye-sensitized solar cells by open-circuit photovoltage decay method. *J. Am. Chem. Soc.* **2004**, *126*, 13550–13559. [[CrossRef](#)] [[PubMed](#)]